11-23-2010

Domain structure-dielectric property relationship in lead-free (1–x)(Bi1/2Na1/2)TiO3–xBaTiO3 ceramics

C. Ma
Iowa State University

Xiaoli Tan
Iowa State University, xtan@iastate.edu

E. Dul'kin
Hebrew University of Jerusalem

M. Roth
Hebrew University of Jerusalem

Domain structure-dielectric property relationship in lead-free (1−x)(Bi1/2Na1/2)TiO3−xBaTiO3 ceramics

Abstract

The domain morphology and crystal structure of (1−x)(Bi1/2Na1/2)TiO3−xBaTiO3 lead-free piezoelectric ceramics were systematically studied with transmission electron microscopy for compositions x=0.04through 0.11. It was found that the ceramics with compositions x<0.06 display a R3csymmetry with ferroelectric domains of ~100 nm forming complex structures at room temperature. Only nanodomains with faint contrast were observed in the compositions of 0.07≤x≤0.09. The presence of weak 1/2 (ooe)superlattice diffraction spots and absence of 1/2 (ooo) ones (o stands for odd and e stands for even miller indices) seem to suggest a P4bm symmetry at room temperature. The morphotropic phase boundary composition x=0.06 showed mixed R3c and P4bm phases. Large lamellar ferroelectric domains with P4mm symmetry were found to dominate in the ceramic of x=0.11. The observed domain structure correlates extremely well with the frequency dispersion of dielectric constant at room temperature and a new concept "relaxor antiferroelectric" was proposed to describe the dielectric behavior of compositions 0.07≤x≤0.09. These results are summarized in a phase diagram for unpoled ceramics in the (1−x)(Bi1/2Na1/2)TiO3−xBaTiO3binary solid solution system.

Keywords

Ceramics, Relaxor ferroelectrics, Dielectrics, Sodium, Transmission electron microscopy, Crystal structure, Phase diagrams, Superlattices, Lead, Ozone

Disciplines

Ceramic Materials | Materials Science and Engineering

Comments

The following article appeared in *Journal of Applied Physics* 108 (2010): 104105 and may be found at http://dx.doi.org/10.1063/1.3514093.

Domain structure-dielectric property relationship in lead-free (1 x) (Bi 1 / 2 Na 1 / 2) TiO 3 x BaTiO 3 ceramics

C. Ma, X. Tan, E. Dul'kin, and M. Roth

Citation: Journal of Applied Physics **108**, 104105 (2010); doi: 10.1063/1.3514093
View online: http://dx.doi.org/10.1063/1.3514093
View Table of Contents: http://scitation.aip.org/content/aip/journal/jap/108/10?ver=pdfcov
Published by the AIP Publishing

Domain structure-dielectric property relationship in lead-free $(1-x)(Bi_{1/2}Na_{1/2})TiO_3$—$xBaTiO_3$ ceramics

C. Ma,[1] X. Tan,[1,a)] E. Dul'kin,[2] and M. Roth[2]
[1]*Department of Materials Science and Engineering, Iowa State University, Ames, Iowa 50011, USA*
[2]*Department of Applied Physics, The Hebrew University of Jerusalem, Jerusalem 91904, Israel*

(Received 14 July 2010; accepted 9 October 2010; published online 23 November 2010)

The domain morphology and crystal structure of $(1-x)(Bi_{1/2}Na_{1/2})TiO_3$—$xBaTiO_3$ lead-free piezoelectric ceramics were systematically studied with transmission electron microscopy for compositions $x=0.04$ through 0.11. It was found that the ceramics with compositions $x<0.06$ display a $R3c$ symmetry with ferroelectric domains of ~100 nm forming complex structures at room temperature. Only nanodomains with faint contrast were observed in the compositions of $0.07 \leq x \leq 0.09$. The presence of weak 1/2 (*ooe*) superlattice diffraction spots and absence of 1/2 (*ooo*) ones (*o* stands for odd and *e* stands for even miller indices) seem to suggest a $P4bm$ symmetry at room temperature. The morphotropic phase boundary composition $x=0.06$ showed mixed $R3c$ and $P4bm$ phases. Large lamellar ferroelectric domains with $P4mm$ symmetry were found to dominate in the ceramic of $x=0.11$. The observed domain structure correlates extremely well with the frequency dispersion of dielectric constant at room temperature and a new concept "relaxor antiferroelectric" was proposed to describe the dielectric behavior of compositions $0.07 \leq x \leq 0.09$. These results are summarized in a phase diagram for unpoled ceramics in the $(1-x)(Bi_{1/2}Na_{1/2})TiO_3$—$xBaTiO_3$ binary solid solution system. © *2010 American Institute of Physics*. [doi:10.1063/1.3514093]

I. INTRODUCTION

Piezoelectric materials are of technological importance because of their wide applications in transducers, actuators, and microelectronic devices.[1–3] Although lead-based perovskites such as $Pb(Zr_xTi_{1-x})O_3$ (PZT) have been the material of first choice for the past five decades due to their excellent piezoelectric performance,[1,2] the toxicity of lead raised serious environmental concerns and the restriction of use of lead in electronic devices has been implemented in environmental legislations in many countries.[3] This has led to intensive worldwide efforts in the search for lead-free ferroelectric ceramics with good piezoelectric properties.

The $(Bi_{1/2}Na_{1/2})TiO_3$—$BaTiO_3$ (BNT–BT) solid solution is one of the most promising and extensively studied lead-free piezoelectric ceramics.[3–7] The high piezoelectric coefficient and low free permittivity make it superior in high-frequency ultrasonic applications and piezoelectric actuators.[4] The optimal piezoelectric property in $(1-x)$BNT–xBT was found at its morphotropic phase boundary (MPB) $x \sim 0.06$, which was believed to separate a rhombohedral ferroelectric phase isostructural with pure BNT ($R3c$) and a tetragonal ferroelectric one isostructural with BT ($P4mm$).[4–6] The investigation of the ferroelectric domain morphology, crystal structure, and their correlation with electrical properties for the BNT–BT system is critical for the understanding of the origin of the electric field-induced strains in these lead-free piezoelectric ceramics. However, systematic studies on such issues are still missing in literature.

$(1-x)$BNT–xBT displays complex dielectric behaviors with strong frequency dispersion. When heated, the room-temperature ferroelectric phase transforms into an antiferroelectric (AFE) one at the depolarization temperature T_d, and the AFE phase further changes to a paraelectric one at T_m.[4,5] The dielectric constant, ε_r, peaks at the temperature T_m around 280 °C. The frequency dispersion in dielectric permittivity vanishes at temperatures several tens of degrees below T_m.[4,5] In literature, T_d is determined from the hump of the temperature dependence curve of loss tangent. However, for many compositions, this hump does not exist in as-sintered unpoled samples. In this case, T_d is determined by the hump in the loss tangent curve in electrically poled samples.[8,9] This alternative approach is highly questionable because it has been reported that the phase structure can be completely altered by the applied electric field during poling, and the change is not reversed after removing the field.[10] Thus the phase diagram for as-sintered ceramics in the virgin state must be different from those determined using the electrically poled ceramics.[4,9] Unfortunately this phase diagram has not yet been reported in literature.

The crystal structure of the AFE phase above T_d was assigned as pseudocubic previously based on x-ray diffraction,[8] implying that the lattice distortion from the parent $Pm\bar{3}m$ cubic perovskite structure is below the detect limit of x-ray diffraction. Neutron diffraction of the base compound $(Bi_{1/2}Na_{1/2})TiO_3$ suggests that the AFE phase should take the $P4bm$ symmetry, with $a^0a^0c^+$ oxygen octahedron tilt and antiparallel displacements between A-site and B-site cations.[11] Phase diagrams of poled $(1-x)$BNT–xBT ceramics show that T_d reaches a minimum at the MPB composition $x=0.06$,[4,9] indicating that the AFE phase is most stabilized at

a)Electronic mail: xtan@iastate.edu.

the MPB. Recent transmission electron microscopy (TEM) studies revealed that the AFE *P*4*bm* phase is present even at room temperature in the form of nanometer-scale platelets embedded in the *R*3*c* matrix in pure $(Bi_{1/2}Na_{1/2})TiO_3$.[12] Considering the fact that this AFE phase is more stabilized in the MPB compositions of $(1-x)$BNT–xBT than in pure $(Bi_{1/2}Na_{1/2})TiO_3$ as mentioned above, it is highly likely that this *P*4*bm* phase is prominent in the unpoled samples with MPB compositions at room temperature. Experimental evidences are needed to confirm this. On the other hand, the nature of this phase is still under debate.[4,5,13] Although the pinched polarization hysteresis loop suggests an AFE behavior,[4,5] the presence of nanodomains without any large ferroelectric domains, and the almost linear elastic behavior rather indicates a relaxor behavior.[13] The verification of the existence of the *P*4*bm* phase in unpoled samples at room-temperature and the determination of its nature are the first step toward understanding the origin of the high piezoelectric performance of BNT–BT.

Associated with the crystal structure and dielectric behavior is the ferroelectric domain morphology. However, domains and their evolution with composition around the MPB in $(1-x)$BNT–xBT has not been systematically investigated with TEM. Limited reports on individual compositions in literature show inconsistent results.[12–20] In the single crystals of 0.97BNT–0.03BT and 0.92BNT–0.08BT, it was claimed that no signs of domains exist.[16] Recently nanodomains of oxygen octahedron tilt were imaged using the dark field technique in BNT–BT ceramics doped with K^+ and Li^+.[17,18] However, we did observe large lamellar ferroelectric domains in a composition of 0.94BNT–0.05BT $-0.01(K_{0.5}Na_{0.5})NbO_3$.[13] These previous studies on scattered compositions can hardly lead to a consistent picture about the evolution of the domain morphology with compositions around the MPB in $(1-x)$BNT–xBT.

The present study is designed to sort these issues out with detailed TEM investigations on a series of compositions in the MPB region. Based on the results, a phase diagram for unpoled $(1-x)$BNT–xBT ceramics is constructed. In contrast to the previously reported phase diagrams,[4,9] an additional phase region exhibiting *P*4*bm* symmetry and nanodomains is revealed within $0.07 \leq x \leq 0.09$ at room temperature. The MPB at $x \sim 0.06$ with the best piezoelectric properties is shown to separate the *R*3*c* and *P*4*bm* phases rather than the *R*3*c* and *P*4*mm* phases.[4,9] Combined with the dielectric study, a new concept "relaxor AFE" is proposed to describe the *P*4*bm* phase with nanodomains.

II. EXPERIMENTAL PROCEDURE

Polycrystalline ceramic samples of $(1-x)$BNT–xBT ($x=0.04$, 0.06, 0.07, 0.09, 0.11) were prepared via a solid state reaction approach. Powders of Bi_2O_3 (≥99.9%, nanopowder, Aldrich), Na_2CO_3 (≥99.9%, Fisher), $BaCO_3$ (≥99.99%, Alfa Aesar), and TiO_2 (≥99.99%, Aldrich) were used as starting materials. Stoichiometric amount of powders were mixed and vibratory milled in ethanol with zirconia mill media for 7 h and then dried. The Na_2CO_3 powder was baked at 200 °C for 15 h and then weighed immediately to ensure stoichiometry. The mixture was calcined at 800 °C for 2 h and then vibratory milled for another 16 h. After drying, the powders were evenly mixed with binder (10 wt % polyvinyl alcohol solution) and then uniaxially pressed into pellets. Following binder burnout at 500 °C, sintering was carried out at 1150 °C for 5 h to obtain dense ceramic pellets. In order to prevent the loss of Bi^{3+} and Na^+, the pellets were buried in a plenty amount of protective powder with the same composition during sintering. The relative density of the sintered pellets is higher than 95% as determined by the Archimedes' method. Scanning electron microscopy examination indicates that the grain size slightly decreases with increasing x. The average grain size is ~3 μm for $x=0.04$, and ~2 μm for $x=0.11$.

The x-ray diffraction experiments were carried out on a PANalytical X'pert PRO MPD x-ray diffractometer with monochromatic Cu $K\alpha$ radiation in the step scanning mode with increments of 0.05° on as-sintered ceramic pellets. With the resolution of the instrument, the results indicated pure pervoskite phases in all ceramics. Then both sides of the pellets were polished and made parallel prior to electrical measurements. Silver paste (Dupont 6160) was fired on at 850 °C for 6 min as electrodes. Dielectric constant and loss tangent under weak electric field above room temperature were measured with an LCR meter (HP-4284A, Hewlett-Packard) in conjugation with a tube furnace during heating at a rate of 3 °C/min. The dielectric characterization below room temperature was performed on a Novocontrol dielectric spectrometer in the step scanning mode with an increment of 5 °C during heating.

As-sintered pellets were mechanically ground and polished down to about 150 μm for TEM specimen preparation. Disks with diameter of 3 mm were ultrasonically cut from the polished slices and the center portion was further thinned to ~5 μm by mechanical dimpling. The dimpled disks were annealed at 250 °C for 2 h to minimize the residual stresses before Ar-ion mill to electron transparency. The ion mill was performed on a Gatan Dual Ion Mill unit (Model 600) at 4 kV, 0.4 mA, and 18° incidence angle. TEM studies were performed on a Phillips CM-30 microscope operated at 300 kV with a Gatan charge coupled device (CCD) camera installed.

III. RESULTS

A. Dielectric characterization

The temperature dependences of the dielectric constant ε_r and loss tangent $\tan\delta$ for unpoled $(1-x)$BNT–xBT ceramics are displayed in Fig. 1. The features of the curves and their variations with the composition are consistent with previous studies.[4–7] The temperature T_m, which is defined as the temperature exhibiting maximum ε_r, shows a weak dependence on composition and is close to 280 °C for all compositions studied. The depolarization temperature T_d is determined by the temperature where the loss tangent shows a hump.[8,9] A strong composition dependence of T_d is seen in Fig. 1. Compositions $x=0.04$, 0.06, and 0.11 show an apparent anomaly in their loss tangent curves and T_d can be easily determined. However, the change in loss tangent as a func-

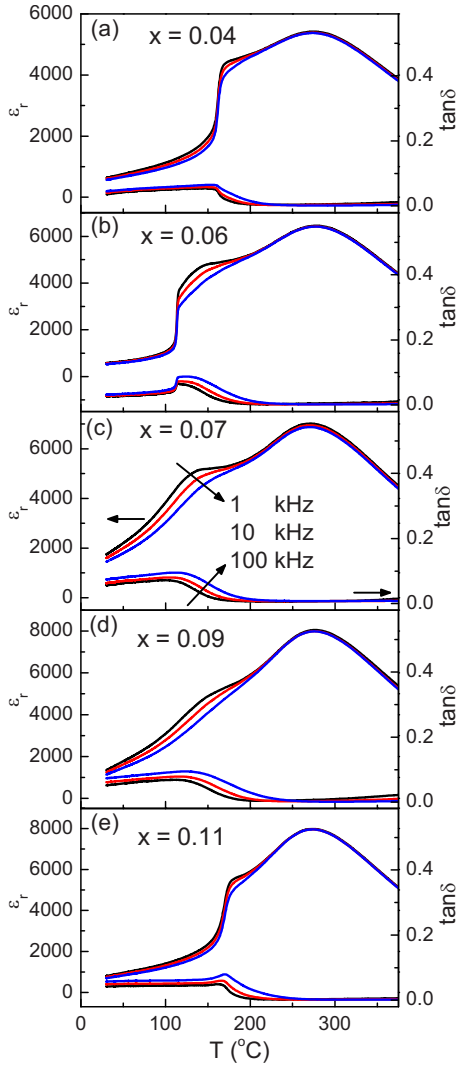

FIG. 1. (Color online) Temperature dependence of the dielectric constant ε_r and loss tan δ for x=0.04, 0.06, 0.07, 0.09, and 0.11 above room temperature measured during heating.

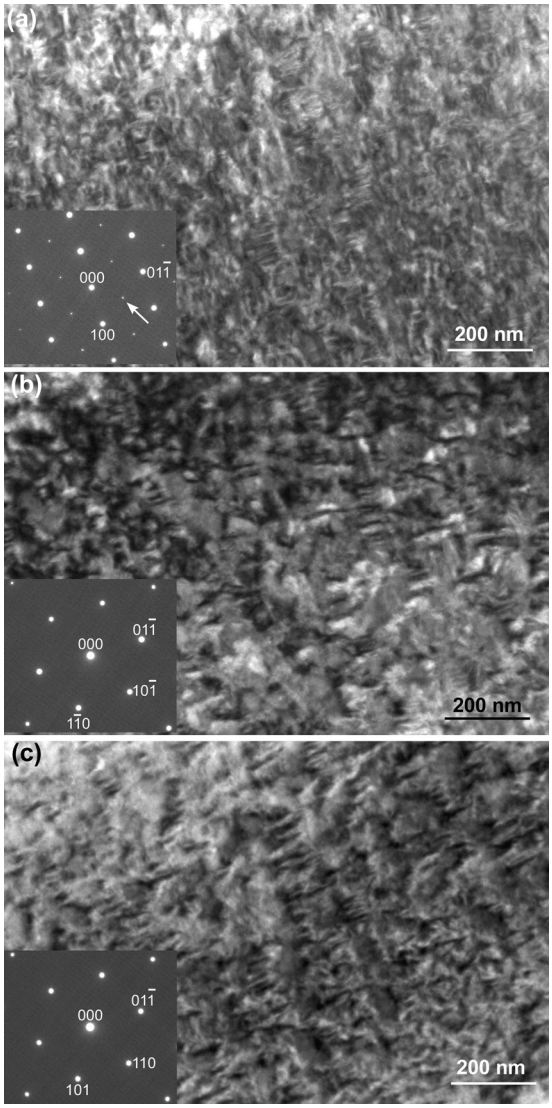

FIG. 2. TEM bright field images of the same area in a representative grain for the composition x=0.04 tilted to (a) [011] zone axis; (b) [111] zone axis; (c) [$\bar{1}$11] zone axis. The insets are the corresponding diffraction patterns.

tion of temperature is very gradual in unpoled x=0.07 and 0.09 ceramics that T_d cannot be identified. It should be pointed out that T_d is not the temperature where a local maximum in ε_r appears. This is most evident in the ceramic x =0.06 where T_d (114 °C) is found about 30 °C below the local maximum in ε_r. In addition to T_d, the frequency dispersion of ε_r and tan δ also display composition dependence. It does not appear until the temperature is above T_d for $x \leq 0.06$ and $x \geq 0.11$ but is present at room temperature and gets stronger with temperature increase for $0.07 \leq x \leq 0.09$. The significant frequency dispersion in the dielectric behavior seems to suggest relaxor characteristics. Unlike the classical relaxor ferroelectrics such as $Pb(Mg_{1/3}Nb_{2/3})O_3$ where frequency dispersion disappears at temperatures slightly above T_m,[21] the frequency dependence in $(1-x)$BNT–xBT ceramics vanishes at a temperature ~30 °C below T_m.

B. TEM study

Previous studies in literature suggest that only perovskite phases with $R3c$, $P4mm$, $P4bm$, and $Pm\bar{3}m$ symmetries need to be considered for $(1-x)$BNT–xBT ceramics at room temperature.[8,9] The $R3c$ perovskite structure is characterized by the presence of 1/2 (ooo) superlattice diffraction spots and the absence of 1/2 (ooe) spots, while the $P4bm$ phase is accompanied by the 1/2 (ooe) superlattice spots without 1/2 (ooo) ones (o stands for odd and e stands for even miller indices).[22,23] These superlattice diffractions are known to be extremely weak in x-ray diffraction. Therefore, selected area electron diffraction (SAED) in TEM offers unique advantages for structural analysis.

Figure 2 displays TEM micrographs and electron diffraction patterns from the same area in a grain with representative features for the composition x=0.04. Ferroelectric domains with sizes around 100 nm are seen when tilted to the [011], [111], and [$\bar{1}$11] zone axes, respectively. Figure 2(a) indicates that the domain walls are along {100} planes. Often times a stack of up to ten domains forms a colony and these colonies made up of differently oriented domains occupy the whole grain in a complex pattern. When tilted to [111] or [$\bar{1}$11] zone axis, {100} domain walls are inclined to the elec-

tron beam. As a result, no sharp contrast of domains is seen. This type of domain morphology does not resemble the previously studied systems including pure $(Bi_{1/2}Na_{1/2})TiO_3$.[12] We refer to this type of domain structure as "complex domain" hereafter. In spite of the different domain morphology, electron diffraction analysis indicates that the crystal structure of composition $x=0.04$ is identical to that of $(Bi_{1/2}Na_{1/2})TiO_3$ at room temperature, which exhibits $R3c$ symmetry with the $a^-a^-a^-$ oxygen octahedron tilt.[11,22,23] This is evidenced by the presence of strong 1/2 (*ooo*) superlattice diffraction spots in SAED patterns of the [011] zone axis [see inset in Fig. 2(a)] and the absence of any superlattice spots in SAED patterns of the [111] or $[\bar{1}11]$ zone axes.

The {100} domains with complex morphology that dominate the composition $x=0.04$ transforms to nanodomains with increasing $BaTiO_3$ content. For the sample with $x=0.06$, ~40% of the grains display a core-shell structure: the core exhibits the complex domains, while the shell consists of nanodomains with faint contrast. The rest of the grains consist of nanodomains only. Figure 3 shows the bright field micrographs and diffraction patterns from the same area of a grain with the core-shell structure recorded along the [011] and [111] zone axes. The SAED pattern from the core exhibits 1/2 (*ooo*) superlattice spots along the [011] zone axis and no superlattice spots along the [111] zone axis, confirming that the core has the same $R3c$ symmetry as the composition $x=0.04$. In contrast, the diffraction pattern from the shell with nanodomains in the same grain displays no superlattice spots along the [011] zone axis, while the 1/2 (*ooe*) spots were observed along the [111] zone axis. This is characteristic of the $P4bm$ symmetry with $a^0a^0c^+$ oxygen octahedron tilt.[12,22] The presence of complex domains within limited volume and the dominating nanodomains seem to be consistent with the dielectric measurement results, which indicate that the AFE phase is stabilized as evidenced by the decrease in T_d from 162 °C in $x=0.04$ to 114 °C in $x=0.06$. The structural instability as evidenced by the coexistence of $R3c$ core and $P4bm$ shell in one grain is in direct support of the excellent piezoelectric properties observed previously in this composition.

For the as-sintered samples with $x=0.07$ and 0.09, only nanodomains were observed. The TEM results from representative grains in these two ceramics are shown in Figs. 4 and 5, respectively. The size of the nanodomains in $x=0.07$ and 0.09 appears slightly larger than that in $x=0.06$. In addition, tendency of texture can also be seen in both compositions when observed along the [011] zone axis. The electron diffraction patterns suggest the crystallographic structure of the nanodomains in these two compositions is identical to that of the shell in the $x=0.06$ composition: weak 1/2 (*ooe*) spots were observed when the grain is tilted to its [111] zone axis and no superlattice spot was detected when tilted to the [011] zone axis. The absence of large domains at room temperature seems to be correlated to the absences of T_d in $x=0.07$ and 0.09 within the temperature range for dielectric characterization shown in Fig. 1.

Further increase in $BaTiO_3$ content to $x=0.11$ leads to a microstructure that is dominated by large lamellar ferroelectric domains. Around 20% of the grains contain a small volume occupied by nanodomains, while the rest exhibit lamellar domains only. Figure 6 shows the TEM results of a grain with both lamellar domains and nanodomains. Similar to the ceramics with $x=0.06$, 0.07, and 0.09, the volume with nanodomains exhibits $P4bm$ symmetry as demonstrated by the presence of 1/2 (*ooe*) spots and the absence of 1/2 (*ooo*) spots. When viewed from the [111] zone axis, most lamellar domains are at edge-on position with sharp domain walls. Figures 6(d) and 6(f) indicate that the domain walls are on {101} planes. No superlattice spot was observed along either [011] or [111] zone axis from the volume with large lamellar domains, indicating no oxygen octahedron tilt is present. These are precisely the characteristic domain features of the $P4mm$ $BaTiO_3$.[24] The coexistence of $P4bm$ nanodomains and $P4mm$ lamellar domains indicates that the composition $x=0.11$ is the one across which the transition from the $P4bm$ to the $P4mm$ phase occurs with increasing x in unpoled $(1-x)$BNT–xBT ceramics.

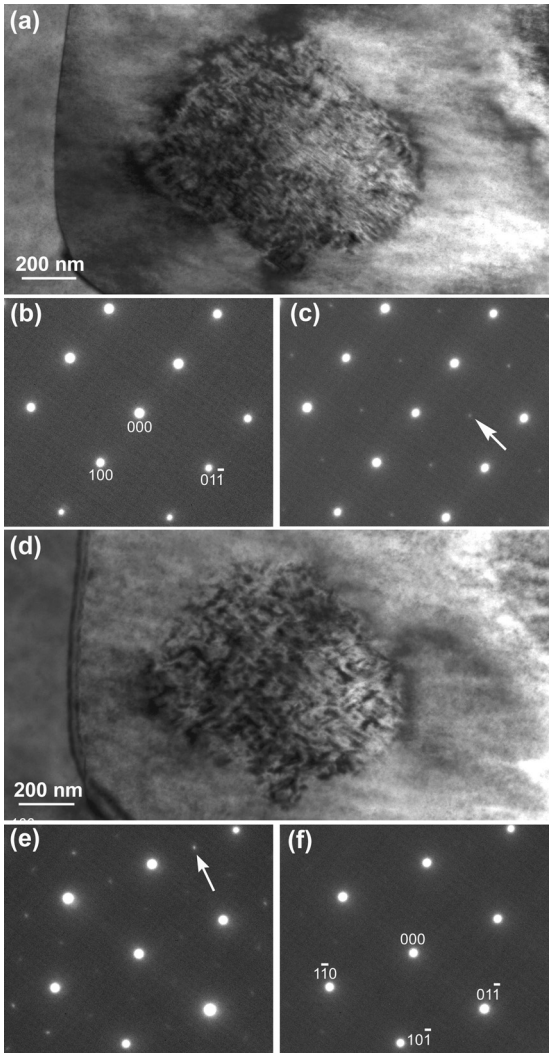

FIG. 3. (a) TEM bright field image of a typical grain with core-shell structure for the composition $x=0.06$ along its [011] zone axis; (b) diffraction pattern of nanodomains along [011] zone axis; (c) diffraction pattern of the complex domain along [011] zone axis; (d) TEM bright field image of the same grain in Fig. 3(a) tilted to its [111] zone axis; (e) diffraction pattern of nanodomains along [111] zone axis; (f) diffraction pattern of complex domains along [111] zone axis.

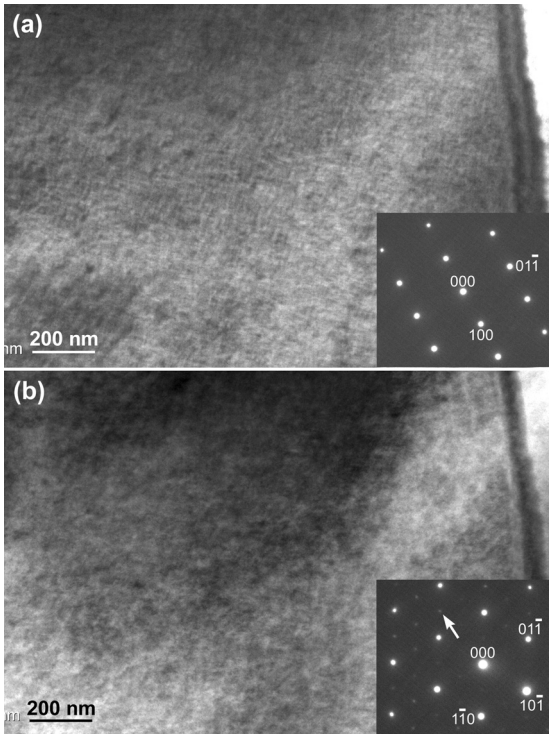

FIG. 4. TEM bright field images of the same area in a representative grain for the composition $x=0.07$ tilted to (a) [011] zone axis; (b) [111] zone axis. The insets are the corresponding diffraction patterns.

IV. DISCUSSION

The evolution of the domain structure in the $(1-x)$BNT–xBT ceramics demonstrates a clear correlation with the dielectric behavior from room temperature up to

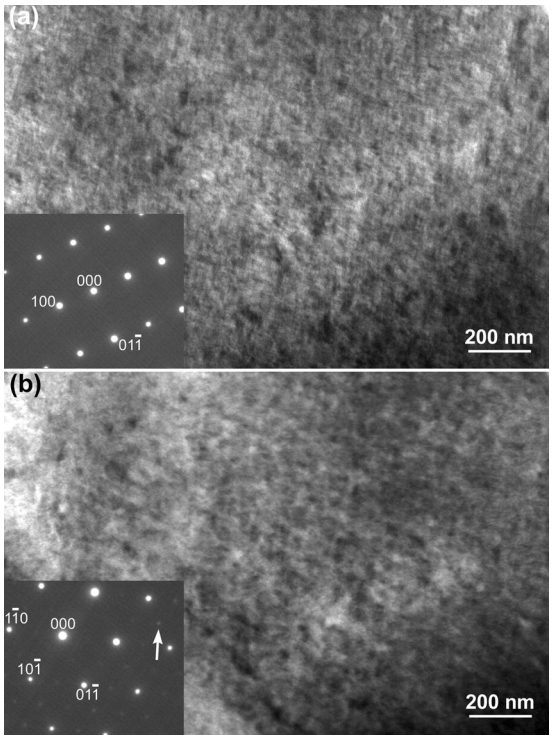

FIG. 5. TEM bright field images of the same area in a representative grain for the composition $x=0.09$ tilted to (a) [011] zone axis; (b) [111] zone axis. The insets are the corresponding diffraction patterns.

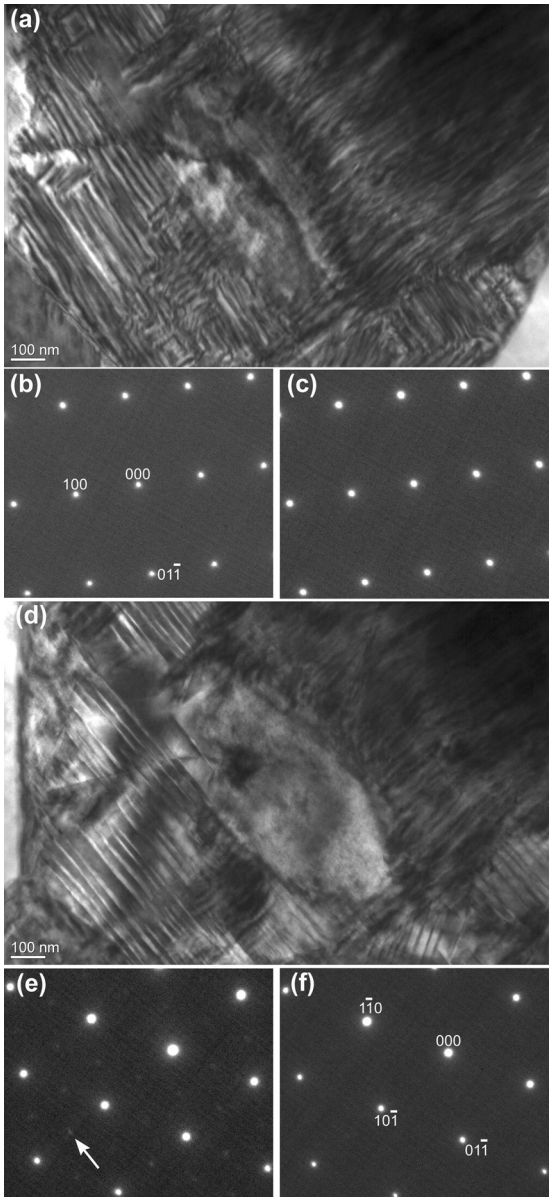

FIG. 6. (a) TEM bright field image of a typical grain exhibiting both lamellar domains and nandomains for the composition $x=0.11$ along its [011] zone axis; (b) diffraction pattern of nanodomains along [011] zone axis; (c) diffraction pattern of the lamellar domain along [011] zone axis; (d) TEM bright field image of the same grain in Fig. 6(a) tilted to its [111] zone axis; (e) diffraction pattern of nanodomains along [111] zone axis; (f) diffraction pattern of lamellar domains along [111] zone axis.

~100 °C: nanodomains correspond to a strong frequency dispersion while regular ferroelectric domains show a weaker frequency dependence. Since the frequency dependence vanishes at ~30 °C below T_m in $(1-x)$BNT–xBT, the dielectric constant above T_m cannot be used to evaluate the relaxation parameter and the diffuseness parameter which were used to characterize Pb-based relaxor ferroelectrics.[25] In order to quantify the frequency dispersion in the dielectric behavior, we define a parameter $\Delta\varepsilon_r$ as

$$\Delta\varepsilon_r = \varepsilon_{r,1\ \mathrm{kHz}} - \varepsilon_{r,100\ \mathrm{kHz}}. \quad (1)$$

The frequency dispersion in the ceramics from room temperature up to ~100 °C can well be represented by $\Delta\varepsilon_r$ at 50 °C. This value is plotted against composition x for

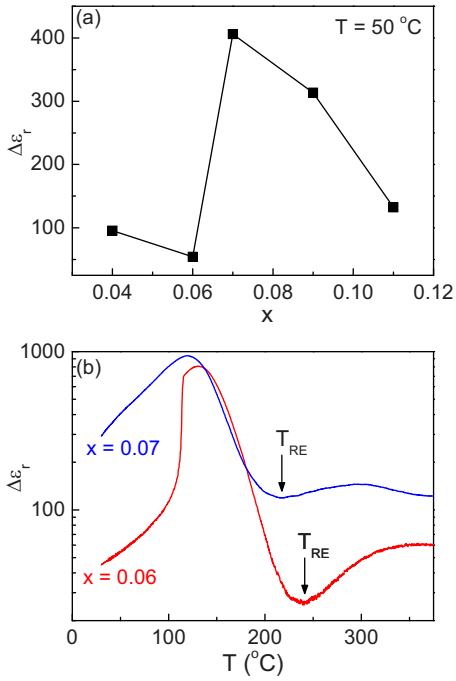

FIG. 7. (Color online) (a) The composition dependence of $\Delta\varepsilon_r$ at 50 °C; (b) the temperature dependence of $\Delta\varepsilon_r$ for $x=0.06$ and 0.07.

$(1-x)$BNT–xBT in Fig. 7(a). It is apparent that compositions $x=0.07$ and 0.09 are outstanding for their large values of $\Delta\varepsilon_r$. This is consistent with their short range order confined within nanodomains.

The frequency dispersion vanishes at a temperature well below T_m for all the compositions studied. However, to identify this relaxor transition temperature for all compositions studied here, the procedure for classical relaxor ferroelectrics, i.e., finding the local maximum in frequency-dependent ε_r, cannot be followed since the frequency dispersion is cut off by T_d in $x=0.04$, 0.06, and 0.11. The temperature for the local maximum in ε_r appears to be below T_d in $x=0.04$ and 0.11 and hence cannot be revealed by the permittivity measurement. The significance of the parameter $\Delta\varepsilon_r$ is also manifested in offering an alternative way to locate this relaxor transition temperature in $(1-x)$BNT–xBT. It is interesting to notice that all the compositions tested display a local minimum in $\Delta\varepsilon_r$ right after the maximum. Figure 7(b) exemplifies the $\Delta\varepsilon_r$ versus T plot for $x=0.06$ and 0.07. We define this unique temperature where $\Delta\varepsilon_r$ is a minimum as T_{RE}, the upper limit for the frequency dependent dielectric behavior. It is clear from Fig. 7(b) that a strong frequency dispersion occurs from room temperature up to T_{RE} for the composition $x=0.07$, while from T_d up to T_{RE} for the composition $x=0.06$. It should be pointed out that the temperature T_{RE} is unique for the dielectric behavior. It does not necessarily correspond to a structural phase transition.

The dielectric characterization above room temperature shown in Fig. 1 does not reveal T_d in compositions $x=0.07$ and 0.09. We speculated that T_d might be below room temperature for these two compositions. Figure 8 displays the temperature dependence of ε_r and tan δ of $x=0.07$ measured during heating from −140 to 100 °C. The dielectric behavior of $x=0.09$ is more or less the same as that of $x=0.07$

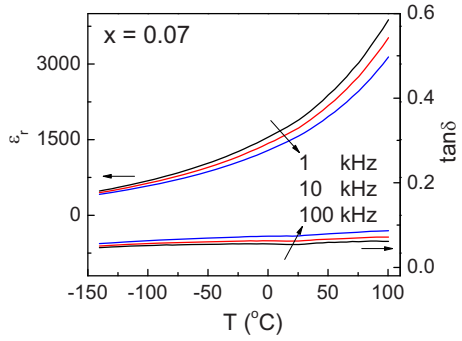

FIG. 8. (Color online) Temperature dependence of the dielectric constant ε_r and loss tan δ for $x=0.07$ from −140 to 100 °C measured during heating.

below room temperature. Neither of them displays any obvious anomaly that can be identified as T_d in the temperature range studied, indicating the phase with the unique relaxor characteristics is still stable at least down to −140 °C in compositions $x=0.07$ and 0.09. However, it is noteworthy that the frequency dispersion is minimum at −140 °C and gradually strengthens as temperature increases. This again resembles the behavior of a relaxor ferroelectric, where the fluctuation of the randomly oriented nanodomains giving rise to the frequency dispersion is suppressed at low temperatures due to the lack of dynamics.[26,27] Since the unique relaxor characteristics of $x=0.07$ and 0.09 are also associated with nanodomains, the low-temperature frequency convergence of dielectric properties seems to suggest these characteristics arise from the dynamic fluctuation of nanodomains.

We have been using the term "relaxor" to describe the dielectric behavior between T_d and T_{RE} for $x=0.04$, 0.06, and 0.11 (this behavior persists from −140 °C up to T_{RE} for $0.07\leq x\leq 0.09$ as demonstrated in Figs. 1 and 8). However, $(1-x)$BNT–xBT has also been historically described as "AFE" above T_d. Supporting evidences exist in literature for both terms.[4,13] We propose a new term relaxor AFE, as oppose to "relaxor ferroelectric" represented by $Pb(Mg_{1/3}Nb_{2/3})O_3$,[27] to reconcile the dispute. In the prototype relaxor ferroelectric compound $Pb(Mg_{1/2}Nb_{2/3})O_3$, the nanodomains are ferroelectric domains, implying that within the volume of individual nanodomains, all the electrical dipoles are parallel and aligned. Relaxor ferroelectric behavior is resulted from randomly oriented and dynamically fluctuating nanodomains.[26] In the case of relaxor AFE as present in $(1-x)$BNT–xBT, we suggest that the displacements of A-site cations (Bi^{3+}, Na^+, Ba^{2+}) are antiparallel to the displacement of B-site cation (Ti^{4+}) within each individual nanodomain, i.e. the nanodomains are of AFE nature. This is supported by the fact that the nanodomained $x=0.07$ and 0.09 display the *P*4*bm* symmetry, which is identical to the AFE phase of the base compound $(Bi_{1/2}Na_{1/2})TiO_3$ existing between 255 and 540 °C with the displacement of Bi^{3+}/Na^+ antiparallel to that of Ti^{4+} and along the [001] direction.[11] However, the AFE ordering in $(1-x)$BNT–xBT below T_{RE} is a short-ranged one confined within each individual nanodomains. Similar to the relaxor ferroelectric $Pb(Mg_{1/3}Nb_{2/3})O_3$ with polar vectors fluctuating among equivalent ⟨111⟩ directions,[26–29] the dynamic fluctuation of the cation displacements along the six equivalent ⟨001⟩ di-

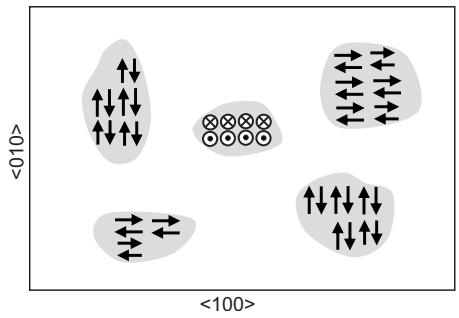

FIG. 9. Schematic diagram of the nanodomains responsible for the observed relaxor AFE behavior in BNT–BT. These AFE nanodomains (the gray islands in the diagram) with the *P*4*bm* symmetry are embedded in the undistorted cubic matrix (the white background in the diagram). The antiparallel arrow pairs denote the cation displacements which fluctuate among the six equivalent $\langle 001\rangle_c$ directions.

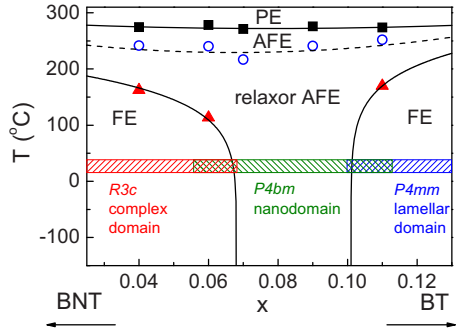

FIG. 10. (Color online) The phase diagram for unpoled $(1-x)$BNT–xBT ceramics. The crystal structure and domain morphology at room temperature are highlighted as shaded boxes. Symbols of solid squares, open circles, and solid triangles represent T_m, T_{RE}, and T_d, respectively, determined from dielectric measurements. PE, AFE, and FE stand for paraelectric, antiferroelectric, and ferroelectric, respectively.

rections in $(1-x)$BNT–xBT leads to the observed frequency dispersion in the dielectric behavior. In addition, as in relaxor ferroelectrics where ferroelectric nanodomains are embedded in a non-polar cubic matrix,[26–29] the AFE nanodomains in $(1-x)$BNT–xBT are also suggested to be embedded in a matrix of undistorted cubic lattice. As a result, only very weak 1/2 (*ooe*) superlattice spots characterizing the *P*4*bm* phase are seen in electron diffraction patterns. A schematic diagram was presented in Fig. 9 to illustrate the concept of relaxor AFE nanodomains in $(1-x)$BNT–xBT.

It has been speculated previously that the competition between long range AFE order and ferroelectric order results in the short-range order relaxor behavior.[30] Following this speculation, adding ferroelectric $BaTiO_3$ to $(Bi_{1/2}Na_{1/2})TiO_3$ introduces the competition between the AFE *P*4*bm* and the ferroelectric *P*4*mm* phase. At compositions $0.07 \leq x \leq 0.09$, the frustration due to the competing long range order reaches a maximum and leads to a relaxor behavior persisting at room temperature. We expect that the long range AFE order will be enhanced at higher temperatures and the normal AFE behavior prevails over the competition. Therefore, the dielectric behavior in $(1-x)$BNT–xBT between T_{RE} and T_m can still be described as AFE. The different relaxor behaviors in $(1-x)$BNT–xBT and $Pb(Mg_{1/2}Nb_{2/3})O_3$ can be attributed to the displacements of different cations for electrical dipoles. In $Pb(Mg_{1/2}Nb_{2/3})O_3$, the displacement of A-site Pb^{2+} along $\langle 111\rangle$ is the primary mechanism for electrical dipoles and the random fields due to disordered B-site cations Mg^{2+} and Nb^{5+} are responsible for the relaxor behavior.[26–29] In $(1-x)$BNT–xBT the situation seems to be reversed. The B-site cation Ti^{4+} is prone to shifting from the center of the oxygen octahedron,[31] and the resulted dipole moment is balanced by the displacement of A-site cations along the opposite direction. Now the random fields come from the A-site disordered cations of Bi^{3+}, Na^+, and Ba^{2+}. It should be noted that the dipole moment resulted from the Ti^{4+} displacement is not fully balanced by that from the A-site cation displacement, leading to a weakly polar ferrielectric order.[11]

We would extend the clear correlation between nanodomains and frequency dispersion in compositions $x=0.07$ and 0.09 to other compositions studied: AFE nanodomains are anticipated between T_d and T_{RE} in ceramics of $x=0.04$, 0.06, and 0.11. At temperatures below T_d in these compositions, the room temperature domain structure (as revealed in Figs. 2, 3, and 6) will be more or less preserved. However, the fraction of volume with nanodomains is expected to increase as the ceramic is heated toward T_d. TEM experiments with a hot stage on the temperature-induced change in domain structure in these three compositions are currently underway to verify this.

The results obtained in this study are summarized in a new phase diagram for unpoled $(1-x)$BNT–xBT ceramics displayed in Fig. 10. The symbols of solid triangles represent T_d, open circles for T_{RE}, and solid squares for T_m. The room-temperature composition dependence of the crystal structure and domain morphology is highlighted as shaded boxes. For compositions $x=0.04$, 0.06, and 0.11, the features for the room temperature domain morphology are expected to persist up to T_d and these fields are denoted as "FE" (stands for "ferroelectric"). For compositions $x=0.07$ and 0.09, the nanodomain morphology observed at room temperature is likely to be preserved until temperatures reach T_{RE}. A similar nanodomain morphology is speculated for the compositions $x=0.04$, 0.06, and 0.11 between T_d and T_{RE}. This field with *P*4*bm* nanodomains is denoted as relaxor AFE (stands for relaxor antiferroelectric) in the phase diagram. For all the compositions between T_{RE} and T_m, a long range AFE order is speculated and is denoted as AFE (stands for antiferroelectric) in the phase diagram. "PE" in Fig. 10 marks the paraelectric phase above T_m.

Compared with the published phase diagrams determined using poled $(1-x)$BNT–xBT ceramics,[4,9] the difference is obvious and yet significant. First of all, there are two composition-induced phase transitions at room temperature in unpoled ceramics within the composition range $x=0.04-0.11$, instead of one in poled ceramics. With increase in x, the long range ferroelectric order (*R*3*c*) changes to a short range AFE order (*P*4*bm*) at around $x=0.06$, and the relaxor AFE phase then transforms to a long range ferroelectric order with the *P*4*mm* symmetry around $x=0.11$. The MPB composition $x=0.06$ previously identified from poled ceramics corresponds to a transition from a ferroelectric *R*3*c* to a relaxor AFE *P*4*bm* phase in unpoled ceramics. Secondly, a new phase transition temperature T_{RE} is defined and in-

cluded. This transition is diffuse and frequency dependent and may not correspond to any structural symmetry change. The decoupling of dielectric response from the crystal structural phase transition has been noticed previously in the base compound $(Bi_{1/2}Na_{1/2})TiO_3$.[4,5,11,14] Thirdly, a new relaxor AFE model is introduced to describe the broad phase region with AFE nanodomains. Under sufficient applied electric fields, two types of electric-field-induced phase transitions, i.e. the relaxor-to-ferroelectric and the AFE-to-ferroelectric, can be expected during the poling process of unpoled ceramics of $x=0.07$ and 0.09 at room temperature. From the previous phase diagrams for poled ceramics,[4,9] a tetragonal ferroelectric phase should be resulted. Indeed recent *in situ* x-ray diffraction confirmed such phase transitions.[10] However, to visualize the evolution of the domain morphology during the phase transition, *in situ* TEM studies with applied electric fields are needed.[20,32,33]

V. CONCLUSIONS

In summary, the composition dependence of domain morphology and crystal structure as well as their correlation with the dielectric behavior are investigated at room temperature in unpoled $(1-x)$BNT–xBT ceramics around the MPB composition. It is found that, for $0.04 \leq x \leq 0.06$, the ceramics are characterized with {100} ferroelectric domains with a length around 100 nm. These domains display the $R3c$ symmetry and form a complex pattern. For $0.06 \leq x \leq 0.11$, nanodomains with short range AFE order are observed. Electron diffraction suggests the $P4bm$ symmetry for these nanodomains. For $x \geq 0.11$, large lamellar {101} domains with $P4mm$ structure are the dominant feature. The composition $x=0.11$ and the previously determined MPB composition $x=0.06$ both display a core-shell grain structure with mixed domain features. The observed domain morphology shows excellent correlation with the dielectric behavior: Regular ferroelectric domains correspond to minimum frequency dispersions in dielectric permittivity while nanodomains lead to strong frequency dispersions.

A new critical temperature, T_{RE}, is defined based on the analysis of the dielectric behavior. Combined with the TEM results, a phase diagram for unpoled $(1-x)$BNT–xBT ceramics to account for different dielectric phases is constructed. We propose that regular ferroelectric domains observed at room temperature will persist up to T_d. The nanodomains are believed to be disrupted AFE domains and are stable up to T_{RE}. The term relaxor AFE is coined to describe the phase region where the ceramic only contains $P4bm$ AFE nanodomains. Since the frequency dispersion in dielectric permittivity vanishes at T_{RE}, we suggest that a long range AFE order exists between T_{RE} and T_m.

ACKNOWLEDGMENTS

This work was supported by the National Science Foundation (NSF) through Grant No. DMR-1037898 and the U.S.-Israel Binational Science Foundation through Grant No. 2006235. TEM experiments were performed at the Ames Laboratory which is operated for the U.S. Department of Energy by Iowa State University under Contract No. DE-AC02-07CH11358.

[1] B. Jaffe, W. R. Cook, and H. Jaffe, *Piezoelectric Ceramics* (Academic, London, 1971).
[2] G. H. Haertling, J. Am. Ceram. Soc. **82**, 797 (1999).
[3] J. Rödel, W. Jo, K. Seifert, E. M. Anton, T. Granzow, and D. Damjanovic, J. Am. Ceram. Soc. **92**, 1153 (2009).
[4] T. Takenaka, K. Maruyama, and K. Sakata, Jpn. J. Appl. Phys., Part 1 **30**, 2236 (1991).
[5] C. Xu, D. Lin, and K. W. Kwok, Solid State Sci. **10**, 934 (2008).
[6] M. Chen, Q. Xu, B. H. Kim, B. K. Ahn, J. H. Ko, W. J. Kang, and O. J. Nam, J. Eur. Ceram. Soc. **28**, 843 (2008).
[7] E. Dul'kin, E. Mojaev, M. Roth, S. Greicius, and T. Granzow, Appl. Phys. Lett. **92**, 012904 (2008).
[8] Y. Hiruma, H. Nagata, and T. Takenaka, J. Appl. Phys. **104**, 124106 (2008).
[9] Y. Hiruma, Y. Watanabe, H. Nagata, and T. Takenaka, Key Eng. Mater. **350**, 93 (2007).
[10] J. E. Daniels, W. Jo, J. Rödel, and J. L. Jones, Appl. Phys. Lett. **95**, 032904 (2009).
[11] G. O. Jones and P. A. Thomas, Acta Crystallogr., Sect. B: Struct. Sci. **58**, 168 (2002).
[12] V. Dorcet and G. Trolliard, Acta Mater. **56**, 1753 (2008).
[13] X. Tan, E. Aulbach, W. Jo, T. Granzow, J. Kling, M. Marsilius, H. J. Kleebe, and J. Rödel, J. Appl. Phys. **106**, 044107 (2009).
[14] V. Dorcet, G. Trolliard, and P. Boullay, Chem. Mater. **20**, 5061 (2008).
[15] G. Trolliard and V. Dorcet, Chem. Mater. **20**, 5074 (2008).
[16] A. N. Soukhojak, H. Wang, G. W. Farrey, and Y. M. Chiang, J. Phys. Chem. Solids **61**, 301 (2000).
[17] C. W. Tai, S. H. Choy, and H. L. W. Chan, J. Am. Ceram. Soc. **91**, 3335 (2008).
[18] C. W. Tai and Y. Lereah, Appl. Phys. Lett. **95**, 062901 (2009).
[19] S. T. Zhang, A. B. Kounga, E. Aulbach, T. Granzow, W. Jo, H. J. Kleebe, and J. Rödel, J. Appl. Phys. **103**, 034107 (2008).
[20] J. Kling, X. Tan, H.J. Kleebe, H. Fuess, W. Jo, and J. Rödel, J. Am. Ceram. Soc. **93**, 2452 (2010).
[21] X. Zhao, W. Qu, X. Tan, A. A. Bokov, and Z.-G. Ye, Phys. Rev. B **79**, 144101 (2009).
[22] D. I. Woodward and I. M. Reaney, Acta Crystallogr., Sect. B: Struct. Sci. **61**, 387 (2005).
[23] A. M. Glazer, Acta Crystallogr., Sect. A: Cryst. Phys., Diffr., Theor. Gen. Crystallogr. **31**, 756 (1975).
[24] H. Hu, H. M. Chan, X. W. Zhang, and M. P. Harmer, J. Am. Ceram. Soc. **69**, 594 (1986).
[25] N. Vittayakorn, G. Rujijanagul, X. Tan, M. A. Marquardt, and D. P. Cann, J. Appl. Phys. **96**, 5103 (2004).
[26] A. A. Bokov and Z.-G. Ye, J. Mater. Sci. **41**, 31 (2006).
[27] L. E. Cross, Ferroelectrics **76**, 241 (1987).
[28] X. Zhao, W. Qu, X. Tan, A. A. Bokov, and Z.-G. Ye, Phys. Rev. B **75**, 104106 (2007).
[29] G. A. Smolenskii, J. Phys. Soc. Jpn. **28**, 26 (1970).
[30] I. W. Chen, J. Phys. Chem. Solids **61**, 197 (2000).
[31] I. Grinberg, M. R. Suchomel, P. K. Davies, and A. M. Rappe, J. Appl. Phys. **98**, 094111 (2005).
[32] H. He and X. Tan, Phys. Rev. B **72**, 024102 (2005).
[33] W. Qu, X. Zhao, and X. Tan, J. Appl. Phys. **102**, 084101 (2007).